APPLICATION OF EPM TO THE SEPARATION OF INCLUSION PARTICLES FROM LIQUID METAL

S. Taniguchi[1], *N. Yoshikawa*[1], *K. Takahashi*[2]

[1] *Graduate School of Environmental Studies, Tohoku University, 6-6-02 Aoba-yama, Aoba-ku, Sendai 980-8579, Japan (s-tanig@mail.kankyo.tohoku.ac.jp)*

[2] *PhD Student, Tohoku University, Now Furukawa Sky Co. Ltd.*

Introduction. Electromagnetic Processing of Materials (EPM) has been widely applied to the continuous casting of steel like EMS and EMBR for the purpose of clean steel production. Recently, effective separation method of non-metallic inclusions from liquid steel is being desired because of the strong demand for higher cleanliness of steel products. Concerning nonferrous metals like aluminum and copper, the situation is quite the same. Especially for the recycling of aluminum, it is needed to remove fine inclusions from molten scrap, which originate in paints. Electromagnetic (em) separation is one of the most promising methods for inclusion removal, which is based on the works done by Leenov and Kolin [1] and Marty and Alemany [2]. Various methods have been proposed to generate em forces in liquid metal: simultaneous imposition of direct current and stationary magnetic field [3]; imposition of alternating current [4]; simultaneous imposition of alternating current and ac magnetic field [5, 6]; imposition of ac magnetic field [7, 8, 9, 10]; imposition of traveling magnetic field [11]. In spite of many researches on em separation, the effect of induced flow of liquid metal on the separation efficiency has not been clarified yet. In the present study, the effect of induced flow on the separation of inclusion particles is investigated from microscopic and macroscopic view points.

1. Principle of em separation. Leenov and Kolin derived a theoretical expression of the force acting on a single sphere suspended in liquid in the case that the electrical conductivity of the sphere (σ_{p}) and liquid (σ_{L}) are different. Their equation is as follows:

$$\mathbf{F}_{\mathrm{p}} = -\frac{3}{2}\frac{\sigma_{\mathrm{L}} - \sigma_{\mathrm{p}}}{2\sigma_{\mathrm{L}} + \sigma_{\mathrm{p}}} V_{\mathrm{p}}\mathbf{F} \tag{1}$$

where $\mathbf{F}_{rmp}$ is the separation force acting on a sphere, V_{P} is the volume of the sphere and $\mathbf{F}$ is the em force given by $\mathbf{J} \times \mathbf{B}$. This separation force does not include the effect of fluid flow around the sphere because the viscous force cancels out totally on the sphere. As inclusion particles are nonconductive compared with the liquid metal in general, σ_{p} is zero in Eq. (1) and the following equation is obtained:

$$\mathbf{F}_{\mathrm{p}} = -\frac{3}{4} V_{\mathrm{p}}\mathbf{F} \tag{2}$$

It should be noted that the direction of the separation force is inverse to the imposed em force. Generally, inclusion particles in liquid metal are small enough to obey the Stokes law of viscous resistance. By equating the force of Eq. (2) with the Stokes force, the following equation is derived.

$$\mathbf{u}_{\mathrm{p}} = -(d_{\mathrm{p}}^2/24\mu)\,\mathbf{F} \tag{3}$$

If the above law is applied, we can realize the em separation of inclusion particles from liquid metal. In the case where the ac magnetic field is imposed alone, the induced em force should be restricted in a skin depth $\left(\delta = (\pi f \mu_e \sigma_e)^{-1/2}\right)$, which becomes thin with increasing frequency, f. In order to enhance the separation, the fluid flow is effective to carry particles from the bulk of liquid to the vicinity of the wall, where a strong em force captures them. On the other hand, too strong flow will prevent the em separation, because a strong fluid-dynamic force overcomes the em force. Such effects of fluid flow have not been understood well yet. In addition, from the microscopic view point, the induced flows around a nonconductive particle may also play an important role especially when the particle is close to the other particle [12, 13, 14, 15, 16]. In this study, the effects of the fluid flow on the em separation of inclusiond from liquid metal are elucidated by numerical simulations and hot metal experiments.

2. Induced fluid flow around nonconductive spheres.

2.1. Equations. Numerical simulations of the em field and fluid flow were performed under the following condition: two nonconductive spheres are suspended in a conductive fluid in which a uniform stationary magnetic field is imposed and the direct electric current is imposed perpendicular to the magnetic field. Equations of the em field and fluid flow are expressed by

$$\nabla^2 \phi = 0 \tag{4}$$

$$\nabla \cdot \mathbf{v} = 0 \tag{5}$$

$$\rho\Big(\frac{\partial \mathbf{v}}{\partial t} + (\mathbf{v}\nabla)\mathbf{v}\Big) = -\nabla p + \mu \nabla^2 \mathbf{v} + \mathbf{F} \tag{6}$$

$$\mathbf{F} = \mathbf{J} \times \mathbf{B}\,, \qquad \mathbf{J} = -\sigma \nabla \phi \tag{7}$$

¿From the calculated pressure and velocities, the forces acting on spheres are obtained by the following equation

$$\mathbf{F}_{\mathrm{p}} = \iint_S \left(p \mathrm{d}\mathbf{S} + \mathbf{T} \cdot \mathrm{d}\mathbf{S}\right) \tag{8}$$

$$\mathbf{T} = \mu\Big(\frac{\partial v_i}{\partial x_j} + \frac{\partial v_j}{\partial x_i}\Big) \tag{9}$$

The electric field was calculated by the use of software ELFIN, which is based on a mixed scheme of a charge simulation method and a surface simulation method. The flow field was calculated by the software FLUENT (ver.5.2).

2.2. Results. Computed velocity distributions around spheres are indicated in Fig. 1. The calculation was performed for three cases, 1, 2 and 3, as shown in the figure. In case 1, the electric current is imposed from left to right and the magnetic field from top to down of the figure. As the current avoids the nonconductive spheres, the component of the current in the right direction weakens near the right and left edges and in the gap of two spheres, and as a result, the em forces decreases there. On the other hand, the current increases in the flank of two spheres that results in a strong em force in this place. Such difference in em forces around spheres generates a complex em flow as seen in case 1 in Fig. 1. For case 2, the flow in the gap of two spheres is opposite to case 1, while the other tendency is almost similar. For case 3, the flow is almost the same as that of a single sphere. From the computed results of the em flow, the force acting on each sphere is calculated and its result is shown in Fig. 2. This figure shows a relationship between the coefficient of Eq.(2) indicated by Gc (0.75 for the case of

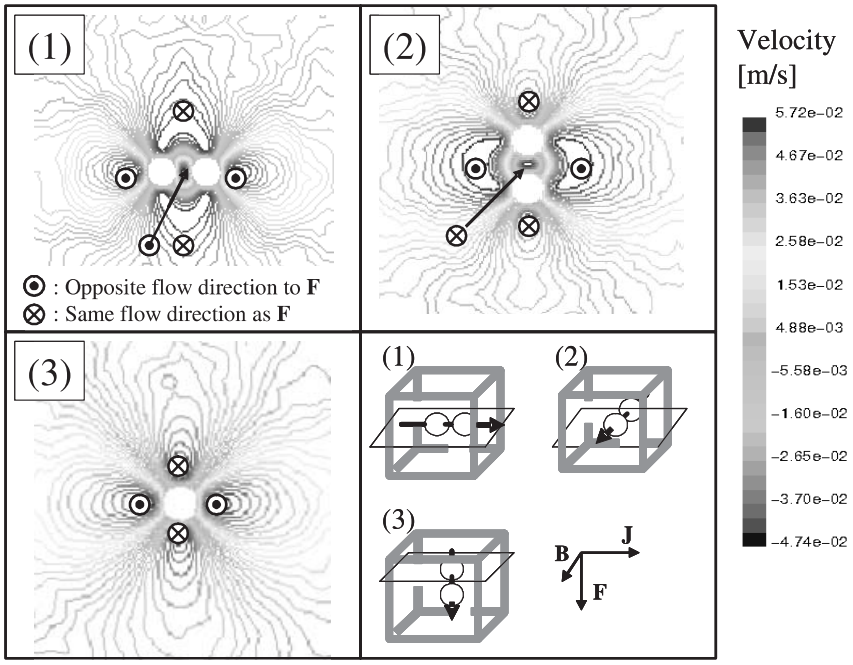

Fig. 1. Arrangement of spheres and results of the em flow.

a single sphere) and the inter-particle distance divided by the particle diameter, $l/2a$. The curves in the figure represent the results without the em flow and the plots represent the results with em flow. For the case without the em flow, the values of Gc of all three cases differ from 0.75 at small $l/2a$, however, they approach 0.75 in large $l/2a$. Comparing the two cases with and without em flow, it is found that the em flow does not influence so much for case 3. However, there can be seen strong effects of the em flow for case 1 and 2. The em flow increases Gc for case 1 and decrease Gc for case 2 and such effects remain even in a large $l/2a$.

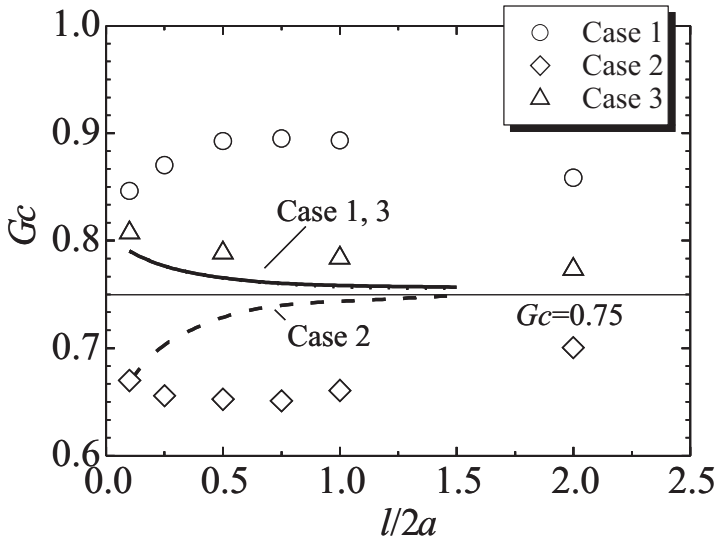

Fig. 2. Relation between Gc and the particle distance (curves: without the em flow, plots: with the em flow).

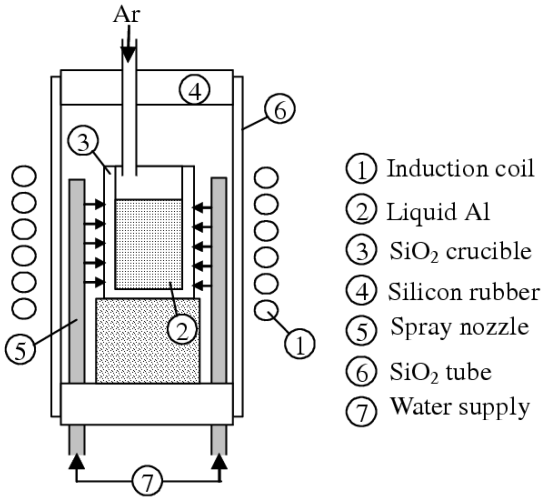

Fig. 3. Experimental apparatus.

3. Em separation of inclusion particles from liquid aluminum.

3.1. Experimental apparatus. Fig. 3 displays an experimental apparatus used for the em separation of SiC particles from Al melt in a high frequency magnetic field. The apparatus is composed of an induction coil, a SiO_2 crucible of 40 mm ID and 100 mm height, spray nozzles for injecting water to the crucible. The experimental procedure is as follows. 0.2 kg of Al is melted in the crucible by induction heating with 30 kHz frequency in Ar atmosphere. After the temperature of Al reaches 1073 K, the coil current is turned off, a piece of the Al alloy including SiC particles (21μm in mean diameter) is put in the melt, the melt is stirred manually during 30 s, and then, the coil current is turned on again. After a prefixed time, the melt is cooled rapidly by the water spray. The solidified aluminum is cut, polished, and observed under an optical microscope to learn the distribution of SiC particles. In the experiment, the following parameters were changed: frequency (3–200 kHz), coil current (42–163 A for 30 kHz), em separation time (8–36 s), particle concentration (1.1–3.0 mass%).

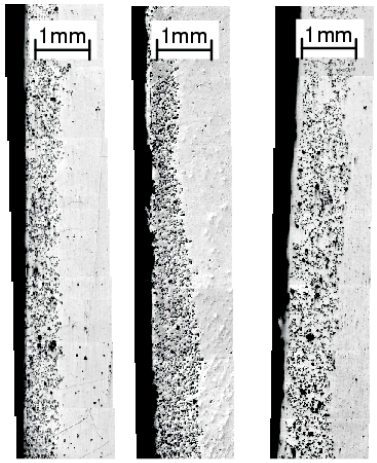

Fig. 4. Separated particle layer near the crucible wall at different times (f = 30 kHz, $I_{\rm rms}$ = 163 A, $C_0 = 1.1\%$).

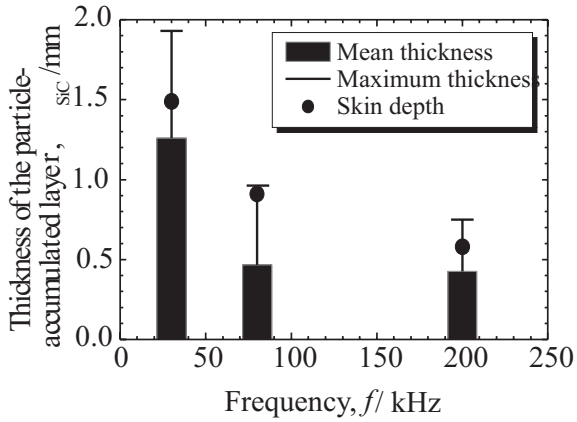

Fig. 5. Thickness of the particle layer compared with the skin depth at different frequencies.

3.2. Experimental results and discussion. The change in thickness of the particle-accumulated layer with the separation time is shown in Fig. 4 at $f = 30$ kHz, $I_{\rm rms} = 163$ A. It is seen from the figure that the em separation proceeds very rapidly and the thickness of the particle layer reaches about 1 mm. It was also found that the thickness of the particle layer increased with increasing particle concentration and was saturated at 3 mass%. It is important to compare the thickness of the particle layer with the skin depth, δ. As the value of δ decreases with increasing frequency, the thickness of the particle layer was measured at different frequencies. The results are shown in Fig. 5, where the mean and maximum thickness of the particle layer is shown together with the values of the skin depth. It is seen from the figure that the thickness of the particle layer roughly corresponds to the skin depth.

From the above results, two conclusions could be derived: the em separation takes place in the vicinity of the crucible wall, where a strong em force exists; particles in the bulk of the liquid are brought to the wall by a liquid flow, which enables a rapid em separation. It should be noted that there is another effect of the liquid flow. The thickness of the particle layer is thin near the free surface and the bottom as shown in Fig. 6. In addition, the particle layer was not formed in the case of 3 kHz. These results strongly suggest that the intensive liquid flow should disturb the em separation.

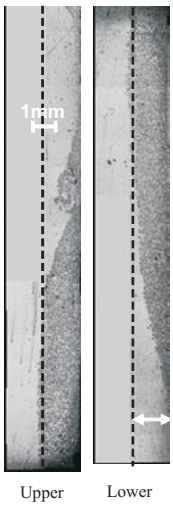

Fig. 6. Particle layer near the wall ($f = 30$ kHz, $t_h = 36$ s, $C_0 = 2.1\%$).

3.3. Numerical simulation of the fluid flow. The Lavers method [17] was applied to calculate em fields in coreless induction furnaces. Taniguchi *et al.* applied this method to obtain magnetic flux density, Joule heat, and em force in liquid metal [18] and obtained a good agreement between calculated and observed values of magnetic flux densities and Joule heat. As this method is analytical, the accuracy is superior to numerical methods especially at high frequencies.

Equations of fluid flow are given in the following, when the general $k-\varepsilon$ model was applied to express the turbulent flow.

$$\frac{1}{r}\frac{\partial r\bar{u}}{\partial r}+\frac{\partial \bar{v}}{\partial z}=0 \tag{10}$$

$$\bar{u}\frac{\partial \bar{u}}{\partial r}+\bar{v}\frac{\partial \bar{u}}{\partial z}=-\frac{1}{\rho}\frac{\partial \bar{p}}{\partial r}+\frac{1}{r}\frac{\partial}{\partial r}\Big(2\nu_{\mathrm{e}}r\frac{\partial \bar{u}}{\partial r}\Big)-\frac{2}{r^2}\nu_{\mathrm{e}}\bar{u}+\frac{\partial}{\partial z}\Big[\nu_e\Big(\frac{\partial \bar{v}}{\partial r}+\frac{\partial \bar{u}}{\partial z}\Big)\Big]+\frac{1}{\rho}\bar{F}_r \tag{11}$$

$$\bar{u}\frac{\partial \bar{v}}{\partial r}+\bar{v}\frac{\partial \bar{v}}{\partial z}=-\frac{1}{\rho}\frac{\partial \bar{p}}{\partial z}+\frac{1}{r}\frac{\partial}{\partial r}\Big[\nu_{\mathrm{e}}r\Big(\frac{\partial \bar{v}}{\partial r}+\frac{\partial \bar{u}}{\partial z}\Big)\Big]+\frac{\partial}{\partial z}\Big(2\nu_{\mathrm{e}}\frac{\partial \bar{v}}{\partial z}\Big)-g+\frac{1}{\rho}\bar{F}_z \tag{12}$$

$$\bar{u}\frac{\partial k}{\partial r}+\bar{v}\frac{\partial k}{\partial z}=\frac{1}{r}\frac{\partial}{\partial r}\Big(r\frac{\nu_{\mathrm{e}}}{\sigma_k}\frac{\partial k}{\partial r}\Big)+\frac{\partial}{\partial z}\Big(\frac{\nu_{\mathrm{e}}}{\sigma_k}\frac{\partial k}{\partial z}\Big)+G-\varepsilon \tag{13}$$

$$\bar{u}\frac{\partial \varepsilon}{\partial r}+\bar{v}\frac{\partial \varepsilon}{\partial z}=\frac{1}{r}\frac{\partial}{\partial r}\Big(r\frac{\nu_{\mathrm{e}}}{\sigma_\varepsilon}\frac{\partial \varepsilon}{\partial r}\Big)+\frac{\partial}{\partial z}\Big(\frac{\nu_{\mathrm{e}}}{\sigma_\varepsilon}\frac{\partial \varepsilon}{\partial z}\Big)+\frac{C_1}{k}\varepsilon\,G-\frac{C_2}{k}\varepsilon^2 \tag{14}$$

where $\bar{u}$ and $\bar{v}$ are the time-averaged flow velocities in r and z directions, ν_{e} is the effective viscosity expressed by Eq.(15), G denotes generation of turbulence expressed by Eq.(16).

$$\nu_{\mathrm{e}}=\nu+\nu_t,\quad \nu_t=C_\mu k^2/\varepsilon \tag{15}$$

$$G=\nu_t\left\{2\left[\Big(\frac{\partial \bar{v}}{\partial z}\Big)^2+\Big(\frac{\partial \bar{u}}{\partial r}\Big)^2+\Big(\frac{\bar{u}}{r}\Big)^2\right]+\Big(\frac{\partial \bar{v}}{\partial r}+\frac{\partial \bar{u}}{\partial z}\Big)^2\right\} \tag{16}$$

Constants included in the above equations are as follows:

$$C_\mu=0.09,\ C_1=1.44,\ \sigma_k=1,\ \sigma_\varepsilon=1.3. \tag{17}$$

The following equations were used for boundary conditions, and the wall function was applied to the velocity distribution near the wall.

$$r=0,\ 0<z<z_1\ :\ \bar{u}=\partial\bar{v}/\partial r=\partial k/\partial r=\partial\varepsilon/\partial r=0\,, \tag{18}$$

$$r=r_1,\ 0<z<z_1\ :\ \bar{u}=\bar{v}=k=\varepsilon=0\,, \tag{19}$$

$$z=0,\ 0<r<r_1\ :\ \bar{u}=\bar{v}=k=\varepsilon=0\,, \tag{20}$$

$$z=z_1,\ 0<r<r_1\ :\ \partial\bar{u}/\partial z=\bar{v}=\partial k/\partial z=\partial\varepsilon/\partial z=0\,, \tag{21}$$

where r_1 and z_1 are the radius and height of liquid metal, respectively. Equations were transformed by stream function and vorticity, and solved by the upwind finite difference method using a non-uniform (24×64) mesh. The property values of liquid Al used in the calculation are as follows: density $\rho=2350$ kgm^{-3}; electric conductivity $\sigma_{\mathrm{e}}=3.8\times10^6$ S$\cdot$m^{-1}; viscosity $\mu=1.11\times10^{-3}$ Pa$\cdot$s.

The results of the velocity distribution are expressed in Figs. 7 *a–d* at different frequencies. In Fig. 7*a* for $f=3$ kHz, four vortices are generated in liquid metal, of which maximum velocity is over 0.3 ms^{-1}. As the frequency increases, the flow becomes calm and unsymmetrical. In the case of $f=30$ kHz shown in Fig. 6*b*, two vortices shrink into the upper wall and bottom and other two predominate in the bulk region. Because of the skin effect, strong flow regions are confined near the upper and lower corners. For the cases of higher frequencies, the velocities in the bulk region decrease remarkably. As seen in Fig.6, the position, where the particle layer is thin, corresponds to the place, where a rapid flow exists.

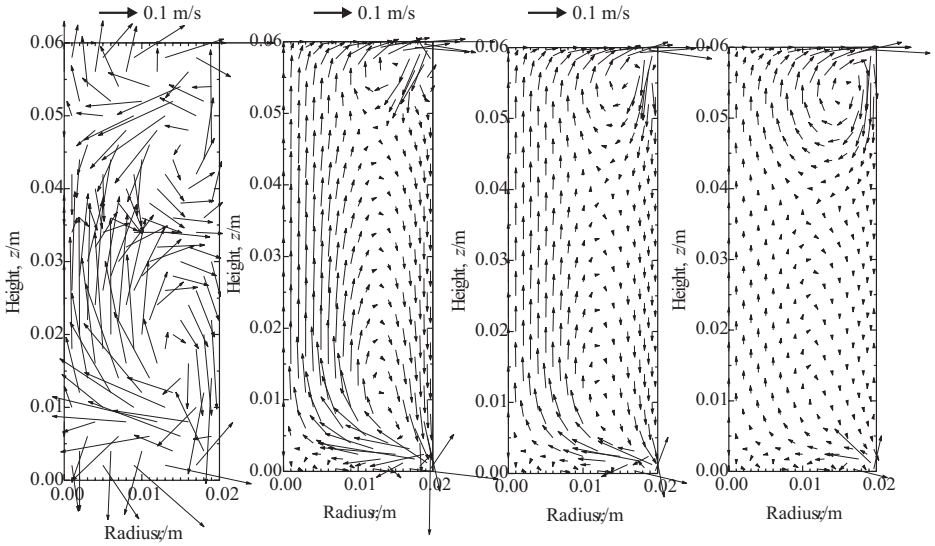

Fig. 7. Computed velocity distribution for various frequencies.

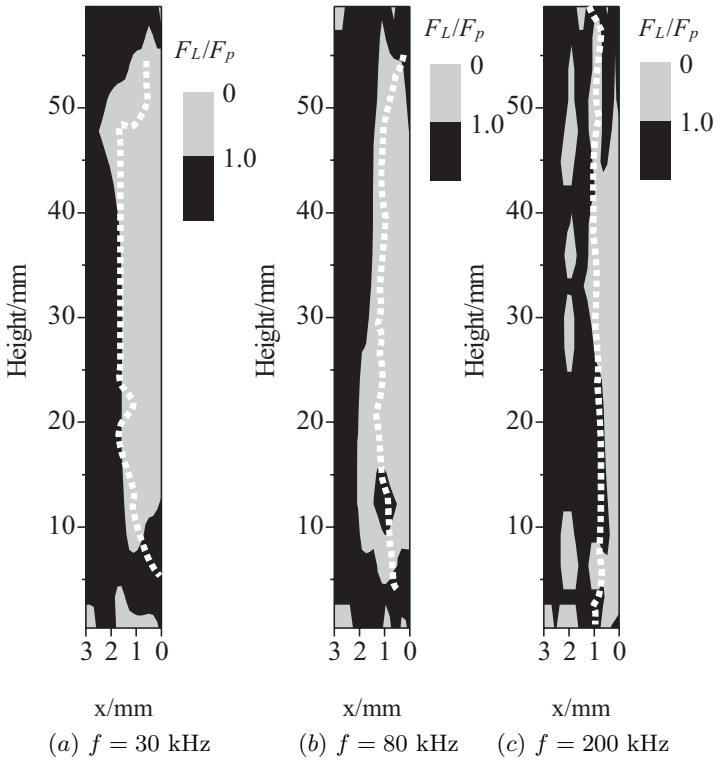

Fig. 8. Comparison between estimated and observed particle layer profile.

3.4. Disturbing effect of the flow on the em separation. The reason why intensive flows interfere the em separation may be attributable to the lift force that takes place in the velocity gradient near the wall. Saffman's theory [19] has often been applied for the lateral migration of particles in laminar flow along a wall. In turbulent flows, Mollinger's empirical equation [20] is available, which was obtained from the direct measurement of the force acting on a particle near the wall. These equations are expressed by the following equations

$$F_{\mathrm{L}}^{\mathrm{S}} = 6.46\,\mu\,\bar{u}_{\mathrm{L}} \left| \frac{\mathrm{d}\bar{u}_{\mathrm{L}}}{\mathrm{d}x} \right|^{1/2} \frac{a^2}{\nu^{1/2}} \tag{22}$$

$$F_{\mathrm{L}}^{\mathrm{M}} = 56.9\,\rho_{\mathrm{L}}\,\nu^2 \left(\frac{a}{\nu^{1/2}} \left| \frac{\mathrm{d}\bar{u}_{\mathrm{L}}}{\mathrm{d}x} \right|^{1/2} \right)^{1.87}, \tag{23}$$

where $F_{\mathrm{L}}^{\mathrm{S}}$ and $F_{\mathrm{L}}^{\mathrm{M}}$ are the lift forces derived by Saffman and Mollinger respectively, μ is the viscosity, ρ_{L} is the liquid density,$\bar{u}_{\mathrm{L}}$ is thw liquid velocity along the wall, a is a particle radius, x is a normal distance from the wall. If this force is stronger than the em separation force, the em separation of particles should be disturbed. In order to estimate the disturbing effect of the lift force, distribution of the lift force was calculated from the computed velocity profile by using Eq.(23). In the calculation, the particle accumulated layer was ignored, which might be acceptable because the volume fraction of particles in the layer was lass than 20%.

Fig. 8 shows the comparison between estimated and observed profiles of the particle layer at various frequencies. In the figure, the gray area indicates the region, where the ratio of lift force to em separation force is less than unity, that is, this area corresponds to the particle accumulated layer. It is seen that the estimated results roughly agree with the observed profiles of the particle layer.

4. Conclusions. The em separation of inclusion particles from liquid metal and the effect of fluid flow on the em separation have been investigated both from microscopic and macroscopic view points. The em flow around two nonconductive spheres suspended in liquid metal was computed under the condition of uniform direct current and stationary magnetic field. The em separation force was found to change with the arrangement of two spheres to the imposed current, magnetic field and em force, and it was affected considerably by the em flow around the spheres. The em separation of SiC particles from molten Al was found to proceed rapidly in a high frequency magnetic field. The particle-accumulated layer formed on the crucible wall was not uniform, that is, it was thin near the free surface and near the bottom of the crucible. Numerical analysis on the em flow was performed to make clear the effect of flow on the em separation. The results indicated that the region, where a strong flow existed, agreed with the position, where the particle layer was thin. A lift force equation was introduced and the region, where the em separation force was larger than the lift force, was calculated. This region was roughly consistent with the particle accumulated layer.

Aqnowlegement. Finally, the authors are grateful to the financial support from the Japanese Ministry of Education, Culture, Sports, Science and Technology, Grant-in-Aid for Scientific Research (2003-2004), and Innovation Plaza Miyagi of JST (Japan Science and Technology Agency) Feasibility Study (2004).

REFERENCES

1. D. Leenov, A. Kolin. *J. Chem. Phys.*, vol. 22 (1954), pp. 683–688.
2. P. Marty, A. Alemany. In *Proceedings of the Symposium of IUTAM* (The Metals Society, London, 1984), pp. 245–259.
3. J. Park, J. Morihisa, K. Sassa, S. Asai. *Tetsu-to-Hagane*, vol. 80 (1994), pp. 389–394. (in Japanese).
4. S. Taniguchi, J.K. Brimacombe. *ISIJ Int.*, vol. 34 (1994), pp. 722–731.
5. A. Alemany, J.P. Argous, J. Barlet, M. Ivanes, R. Moreau, S. Poinsot. French Patent No.80400 4430, (1980).
6. S. Taniguchi, A. Kikuchi. In *Proceedings of the 3rd International Symposium on Electromagnetic Processing of Materials, EPM2000* (Nagoya, Japan, 2000), pp.315-320.
7. F. Yamao, K. Sassa, K. Iwai, S. Asai. *Tetsu-to-Hagane*, vol. 83 (1997), pp. 30–35. (in Japanese).
8. N. El-Kaddah, A.D. Patel, T.T. Natarajan. *JOM*, vol. 47 (1995), pp. 46–49.
9. D. Shu, B. Sun, K. Li, Z. Xu, Y. Zhou. *ISIJ Int.*, vol. 42 (2002), pp. 1241–1250.
10. K. Li, J. Wang, D. Shu, T. Li, B. Sun, Y. Zhou. *Materials. Letter*, vol. 56 (2002), pp. 215–220.
11. Y. Tanaka, K. Sassa, K. Iwai, S. Asai. *Tetsu-to-Hagane*, vol. 81 (1995), pp. 1120–1125. (in Japanese).
12. T. Ogasawara, N. Yoshikawa, S. Taniguchi, T. Asai. In *Proceedings of the 4th International Symposium on Electromagnetic Processing of Materials, EPM2003* (Lyon, France, 2003), pp. 379-384.
13. T. Ogasawara, N. Yoshikawa, S. Taniguchi, T. Asai. *ISIJ Int.*, vol. 43 (2003), pp. 862–868.
14. T. Ogasawara, N. Yoshikawa, S. Taniguchi, T. Asai. *Mater. Trans. B*, vol. 35 (2004), pp. 847–855.
15. D. Shu, B. Sun, J. Wang, K. Li, Z. Xu, Y. Zhou. *Metall. Mater. Trans. B*, vol. 31 (2000), pp. 1527–1533.
16. D. Shu, B. Sun, J. Wang, K. Li, Z. Xu, Y. Zhou. *Metall. Mater. Trans. B*, vol. 31 (2000), pp. 1535–1540.
17. J.D. Lavers. Ph.D. Thesis, University of Toronto,1970.
18. A. Kikuchi, S. Taniguchi, T. Tadaki, S. Maeda. In *Proceedings of a Symposium of the International Union of Theoretical and Applied Mechanics* (Cambridge, UK, 1982), pp. 79-92.
19. P.G. Saffman. *J. Fluid Mech.*, vol. 20 (1965), pp. 385–400; vol. 31 (1968), p. 624.
20. A.M. Mollinger, F.,T.,M. Nieuwstadt. *J. Fluid Mech.*, vol. 316 (1996), pp. 285–306.